Vol. 91 (1997) *ACTA PHYSICA POLONICA A* No. 3

SCANNING TUNNELING SPECTROSCOPY SENSITIVE TO LAYER STRUCTURE OF BSCCO

M. Aleszkiewicz, P. Aleszkiewicz and J. Rauluszkiewicz

Institute of Physics, Polish Academy of Sciences
Al. Lotników 32/46, 02-668 Warszawa, Poland

(Received August 7, 1996; revised version December 16, 1996)

Scanning tunneling microscopy images and scanning tunneling spectroscopy characteristics were measured at 4.2 K in liquid helium bath on the cleaved in air a–b surface of $Bi_2Sr_2CaCu_2O_8$ (BSCCO-2212). Electronic densities of states and superconductivity parameters Δ and Γ evaluated from dI/dV characteristics depend on tip–sample distance s: with shortening of the distance s superconducting gap structure becomes more distinct, i.e. Δ increases and Γ decreases. We explain this phenomenon as a non-vacuum tunneling, where for longer s tunneling electrons reach only the surface contamination layer on non-metallic BiO top-surface layer, whereas for shorter s tunneling electrons penetrate also deeper lying CuO layers reflecting their superconducting properties. The dependence of Δ on s is evaluated. This result allows to understand better the non-vacuum scanning tunneling microscopy imaging: by adjusting properly the tip–sample distance one can select suitable local density of states contributing dominantly to the scanning tunneling microscopy images taken on BSCCO.

PACS numbers: 74.72.Hs, 61.16.Ch, 68.65.+g

1. Introduction

Since its discovery by Binnig and Rohrer [1] STM (scanning tunneling microscopy) has opened many new areas in surface science, technology and engineering [2]. Because the tunneling current in STM imaging is sensitive to surface electron density of states (DOS), resulting raw images are in general pseudo-topographic. For their interpretation an independent measurement of local DOS is necessary. This is the intention of STS methods. An illustration of STS possibilities is the paper by Feenstra et al. [3].

In STS measurements the DOS can be deduced from examination of dI_t/dV_t curves taken either in desired spots on an STM image or registered for all pixels simultaneously with STM data (e.g. the so-called atomic site tunneling AST [4],

or current imaging tunneling spectroscopy CITS [5]), depending on physical requirements. Recording of $\{\mathrm{d}I_\mathrm{t}(V_\mathrm{t}, s, x, y)\}/\mathrm{d}V_\mathrm{t}$ characteristics for all pixels of an image provides sometimes a flood of data difficult for reasonable analysis.

The STM image is very sensitive to surface purity. As a rule, proper STM images can be obtained only in UHV conditions on the clean surfaces free of physical and chemical contaminations. However, there are some materials with surfaces chemically inert in air (e.g. noble metals, graphite), which can be investigated in ambient atmosphere. From the great amount of high-T_c superconductors (HTSC) the $Bi_2Sr_2CaCu_2O_8$ (BSCCO-2212) belongs to this class and is suitable for STM measurements due to its layer structure

.../–BiO–SrO–CuO–Ca–CuO–SrO–BiO–/...

and due to easy cleaving in the van der Waals bonded a–b plane between two adjacent BiO layers, which are chemically inert. The cleaved surface is thought to be covered with BiO monoatomic layer. Recently, two kinds of surfaces measured under the same tunneling conditions (i.e. tunneling junction resistivity) with two different types of tunneling characteristics (semi- and superconducting) were recognized as a result of cleaving [6, 7]. Therefore cleaving which opens a CuO layer takes probably place in some cases [6]. Another explanation of the same phenomenon is that in some cases the topmost CuO layer is nonsuperconducting due to off-stoichiometric composition or to presence of defects [7]. In general, lattice structure, stoichiometry (e.g. oxygen content) and electronic properties of a surface may differ substantially from those in a bulk. In addition, very short coherence length, inhomogeneity of material and extremely local nature of electronic structure demand special cautions in analysis of raw STM results. The STS methods are here recommended.

The dependence of STS characteristics on tip–sample distance measured on BSCCO was analysed and interpreted by Shih et al. [8] in terms of distribution of tunneling voltage V_t in multiple vacuum and BiO–SrO barrier. Wolf et al. [9] have measured simultaneously STM images and the $\mathrm{d}I_\mathrm{t}/\mathrm{d}V_\mathrm{t}(s, x, y)$ maps on BSCCO at 4.2 K. They interpret the superconducting DOS structures observed on the uppermost BiO layer as a superconductivity induced in BiO by proximity effect from deeper CuO planes.

We report the experimental results of STS studies on the a–b plane of BSCCO single crystals in superconducting state aimed to better understanding and interpretation of their STM images on BSCCO and to observation how the superconducting STS parameters Δ and Γ are influenced by the varied tip–sample distance.

2. Experiment

The low temperature scanning tunneling microscope (LT-STM) used in our STM/STS measurements is in principle similar in construction to that of Fein et al. [10]. It was inserted into a helium cryostat just into a helium storage vessel, where the STM head with a mechanically cut PtRh tip was immersed directly in liquid helium. STM images were registered in constant current mode. STS characteristics $I_\mathrm{t}(V_\mathrm{t}, s)_{x,y=\mathrm{const}}$ were recorded in selected spots on previously scanned STM images. The tip–sample distance s was adjusted by varying the tunneling

current I_t at constant V_t or varying the tunneling voltage V_t at constant I_t when the feedback was active. Each analyzed characteristic was an average from 300 measured curves.

Single crystals of $Bi_2Sr_2CaCu_2O_8$ (BSCCO-2212) were grown by the floating zone method in the optically heated furnace. The critical temperature T_c estimated from resistivity measurements was 85 K. Samples of dimensions approximately $2 \times 2 \times 1$ mm allowed to select a–b crystallographic planes and appropriately break the sample. Fresh a–b surfaces were opened by cleaving in air with the aid of an adhesive tape just prior to mounting it into the STM head.

The dI_t/dV_t characteristics (conductivity curves) were calculated from measured $I_t(V_t)$ curves by numerical differentiating.

The background conductance was parabolic at bias up to |100 mV|. Characteristics measured under tunneling conditions where the tip was kept near enough to the sample showed very distinct gap features. Normalization procedure made them also visible on curves taken relatively far away from the sample and made possible showing easy to recognize gap features on all curves in the same scale.

Curves were normalized by subtracting background parabolas, which has the physical meaning of separating normal- and superconducting state conductivity. The resulting pure superconducting data were fitted by the Dynes function

$$F_{\mathrm{Dynes}}(E, \Delta, \Gamma) = \frac{N_s(E)}{N_n(E)} = \mathrm{Re}\left(\frac{E - i\Gamma}{\sqrt{(E - i\Gamma)^2 - \Delta^2}}\right),$$

where $N_s(E)$ is the density of electron states of quasi-particles in the superconducting state, $N_n(E)$ — the density of states in non-superconducting state, Δ is the energy gap and Γ is the damping rate: $\Gamma = h_{\mathrm{Planck}}/2\pi\tau$, τ — the lifetime of the quasi-particle [11]. In this way two best fitting parameters were obtained for each dI_t/dV_t curve. Dynes' model fits quite well to experimental curves. The model relies on the assumption that the s-wave symmetry is valid, although the question about the symmetry as well as the origin of pairing in HTSC is still open. Moreover, $d_{x^2-y^2}$-wave pairing is rather favored than s-wave in some experiments [12, 13] and calculations [14]. Besides Dynes' model there exists several other procedures determining superconducting gap, but in all calculations resulting gap value is about 20% smaller than that obtained from the position of the peaks [15].

In the region outside the superconducting gap the derivative dI_t/dV_t was fitted to a parabola. Three coefficients of these background parabolas depend on three tunneling barrier parameters: barrier width, average barrier height and asymmetry of the barrier height, but the problem of calculating the barrier parameters in the case of STM junctions is not solved yet. The Simmons formulae [16, 17] valid for planar junctions were used, which give the coefficients of conductivity parabolas as functions of barrier parameters. Since these formulae assume non-zero junction area they could not be directly applied to STM junctions — therefore calculated barrier widths s are given in arbitrary units.

Having a set of superconductivity gap parameters for successively varied tip–sample distance s we were able to plot the dependence between superconducting gap value Δ on barrier width s.

3. Results

Figure 1 presents four sets of dI_t/dV_t versus V_t characteristics measured in the range $-0.15\ \text{V} < V_t < 0.15\ \text{V}$ for four various tip–sample distances s indicated in the figure. The curves are not normalized in this figure. Distances indicated in Fig. 1 (as well as in Figs. 2 and 4) are related to the smallest distance in each set of measurements, because the absolute values of s are not known. The spectra, drawn in the same scale indicated in the figure, are arbitrarily displaced vertically for clarity and show only the relative magnitude. For the shortest tip–sample distance s ($s = 1$) the well pronounced superconducting gap, superimposed on parabolic background corresponding to N-I-N tunneling conductivity, is visible. For greater s curvatures of parabolas decrease systematically and the superconducting gap structure vanishes — the parabola of tunneling conductivity is going to be flat indicating higher tunneling resistivities. Beside superconducting structures some additional structures at higher biases V_t are also present on all characteristics. They can indicate the presence of some inelastic tunneling processes, but their origin is not discussed in this paper.

Figure 2 illustrates another set of unnormalized dI_t/dV_t versus V_t characteristics taken under constant tunneling voltage 100 mV, presented as a quasi-three-dimensional drawing. On the horizontal axis there are the voltage (independent variable) and values of tunneling current at which it was stabilized (tunneling current was varied from 100 nA down to 5 nA). Density of states of BiO plane, whose semiconducting gap is typically 70–100 mV [18], is non-zero under this voltage. Therefore non-superconducting part of conductivity should play important role

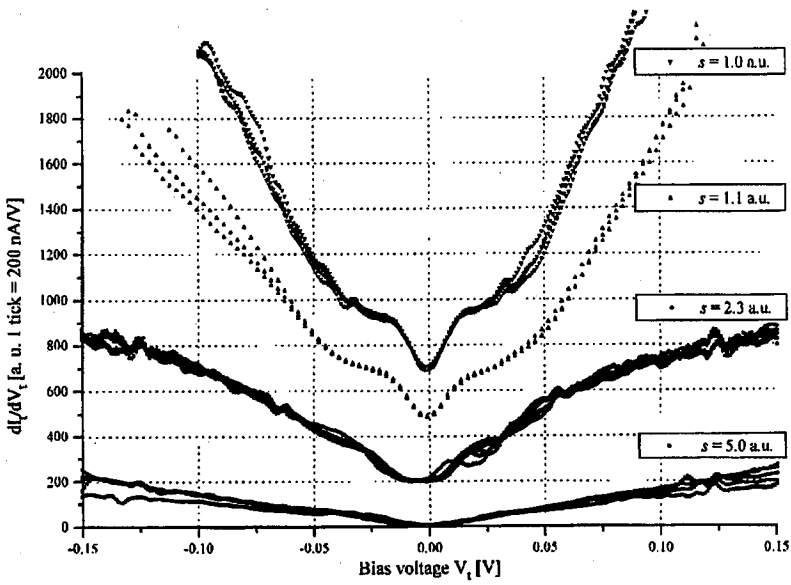

Fig. 1. Sets of dI_t/dV_t vs. V_t on BSCCO-2212 for four different tip–sample distances s. s is given in arbitrary units [a.u.] related to its smallest value.

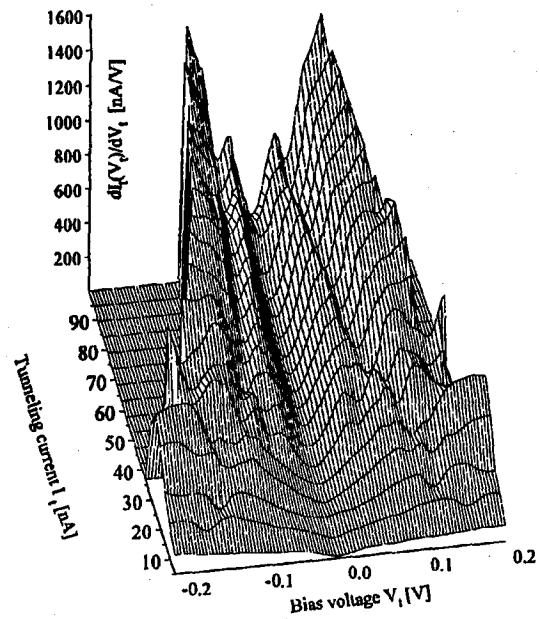

Fig. 2. dI_t/dV_t vs. V_t characteristics presented as the quasi-three-dimensional drawing: on the horizontal axis perpendicular to the plane of figure there are the values, at which the tunneling current was stabilized (tunneling current was varied from 100 nA down to 5 nA at tunneling voltage 100 mV).

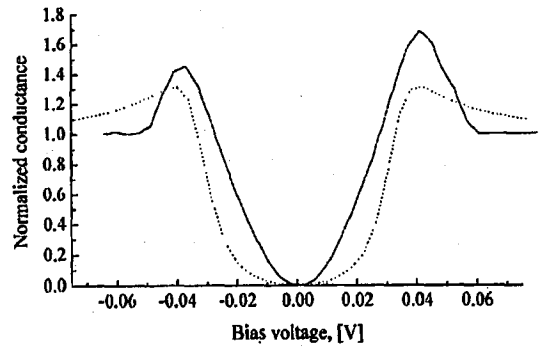

Fig. 3. An example of a shape of a normalized experimental curve (solid line) compared to its Dynes' function fit (dotted). The experimental data reveal more states in the gap.

and be well visible. For short tip–sample distances s, i.e. for large tunneling current, the superconducting gap structures are well pronounced. With the increase in s i.e. in the low current limit the structure gradually vanishes being invisible for large s.

Figure 3 shows an example of a normalized experimental curve with its Dynes' function fit. Compared with broadened BCS function the experimental

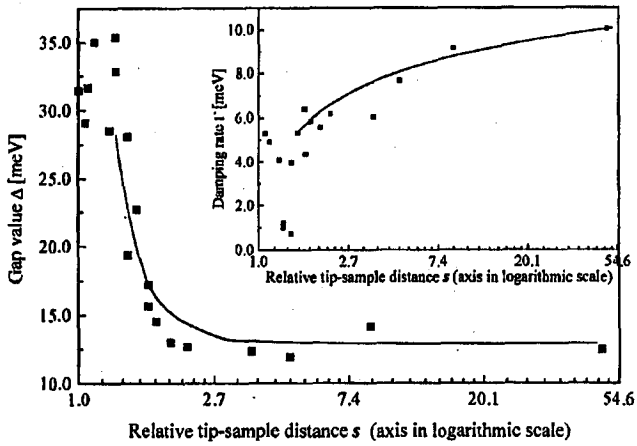

Fig. 4. The dependence of superconducting gap Δ on the tip–sample distance s and the damping rate Γ on s (in the inset). Solid lines are drawn as a guide for the eye.

data reveal more states in the gap than predicted by the isotropic BCS theory, as indicated by other authors, too [7].

From the parabolic region of the dI_t/dV_t versus V_t characteristics the barrier widths were estimated and from the superconducting gap structures on the normalized dI_t/dV_t versus V_t characteristics the parameters Δ and Γ were extracted using procedures as explained above. Figure 4 presents the dependence of Δ on s as a result of these calculations. Increase in Δ while decreasing s is evident. For short distances s values of Δ belong to the region between 25–29 meV and do not systematically change further. Scattering of the results is caused by the fact that each curve belongs to an independent measurement following the surface scan. The dependence of Γ on s (shown in the inset to Fig. 4) is just opposite, i.e. Γ decreases simultaneously with s. Exposing of superconducting structure on subsequent conductivity curves has therefore two reasons, because both superconducting parameters change.

4. Discussion

The layered structure of BSCCO is well known and confirmed in various experiments including that of STM/STS. From very great deal of published STS measurements the values of the most important superconducting parameters Δ and Γ have been deduced, in general very scattered and inconsistent. This great inconsistency in tunneling data results from not precise enough determination of material structure at the surface, from its unknown surface condition (purity), sometimes from not properly performed STS measurements and from differences in methods of extracting gap values from the data. Recently reported results performed on samples cleaved in high vacuum conditions show that under proper conditions pure vacuum tunneling occurs [19]. Curves with flat, ohmic conductance and gap value independent of tip–sample distance are obtained. These curves scale with changes of junction resistivity i.e. tip to sample distance. It was found that other behavior does not reveal intrinsic properties of HTSC [7]. Two other kinds

of tunneling can occur and are often false understood as vacuum tunneling. Linear background at high bias is typical of point contact tunneling. This case occurs if the tip is approached too close to the sample. The other kind of non-vacuum tunneling is tunneling through contaminated junction, where conductance curve has parabolic background. These both cases can be recognized by the junction resistivity, which in case of point contact tunneling is of the order of kΩ, and in the case of tunneling through contaminated junction is similar to the resistivities occurring in vacuum tunneling, i.e. several up to several hundreds MΩ. In our case, when experiments were performed in liquid helium bath on the sample cleaved in air, the occurrence of parabolic background is easy to understand. In order to exclude the possibility that an accidental point junction was formed we examined junction resistivity for data in Fig. 2 in several ways. The wide applied in literature junction resistivity calculated as a ratio of tunneling voltage to tunneling current under which the topographical image was scanned, was varied between 20 MΩ down to 1 MΩ. Static resistivity i.e. current to voltage ratio as measured in $I(V)$ characteristics was 10 down to 1 MΩ outside the gap (at 75 mV). Dynamic resistivity i.e. the inverse of $\mathrm{d}I/\mathrm{d}V$ was 0.9–9 MΩ (at 75 mV). Such high resistivities would not occur if the tip was driven into the sample as a result of improper stabilization of tunneling parameters. Another indication for good quality of our junctions is the absence of large conductance at $V = 0$. In both above described non-vacuum junctions broadening of gap structure occurs. It is probably a result of inelastic processes in surface layer and layers situated above CuO layer which is responsible for superconducting properties of the HTSC [20]. Using the barrier model of tunneling junction on the a–b surface of BSCCO described by Shih [8] and assuming constant penetration depth of tunneling electrons one can expect that in particular case of non-vacuum tunneling experiments for different tip–sample distances s the measured DOS corresponds to subsequent contamination, BiO, SrO and CuO layers. Thus the proper adjustment of s (by varying I_t and V_t) influences substantially the STM image and should be taken into consideration in its interpretation.

The reversal relation between Δ and Γ deduced from our non-vacuum STS measurements with variable s reflects also the rule that the quality and accuracy of Δ measurements by the STS technique are also sensitive to proper adjustment of s (gap smearing). For larger s the tunneling electrons do not reach exactly the superconducting CuO sublayer and reflect partially the properties of non-metallic sublayers with probable superconductivity induced by the proximity effect. For s large enough we would not see any reminders of superconductivity on the parabolic shape of $\mathrm{d}I_\mathrm{t}/\mathrm{d}V_\mathrm{t}$ versus V_t curves. Thus a great diverseness of results in Δ measurements by the STS reported so far on the surfaces of high-T_c superconductors, at least on BSCCO, is due to the fact that the regions reached by tunneling electrons are not controlled precisely and wide variety of results due to extrinsic barrier-related effects is observed.

5. Summary

The STS characteristics measured at 4.2 K in liquid helium bath on the cleaved in air a–b surface of BSCCO-2212 single crystals indicate that the shapes and structures of tunneling conductivity $\mathrm{d}I_\mathrm{t}/\mathrm{d}V_\mathrm{t}$ versus V_t depend evidently on

the tip–sample distance s. This effect is caused by the surface contamination layer on BSCCO and by the limited penetration depth of tunneling electrons. For larger s tunneling electrons reach only contaminated non-metallic BiO top-surface layer, whereas for smaller s tunneling electrons penetrate deeper lying CuO layers reflecting their superconducting electron densities of states. For intermediate ranges of s the values of Δ are not correct, they do not correspond to pure CuO superconducting state.

It follows from our results that the adjustment of tip–sample distance s by stabilization of proper values of V_t and I_t is of great importance in measurements in non-UHV conditions i.e. for interpretation of STM images as well as for evaluation of intrinsic superconducting gap Δ.

Acknowledgments

Dr. J. Fink-Finowicki is greatly acknowledged for supplying BSCCO single crystals. This work is partially supported by the Committee for Scientific Research under grant No. 2.P302.007.06.

References

[1] G. Binnig, H. Rohrer, *IBM J. Res. Dev.* **30**, 335 (1986); G. Binnig, H. Rohrer, Ch. Gerber, E. Weibel, *Appl. Phys. Lett.* **40**, 178 (1982).

[2] H. Rohrer, *Jpn. J. Appl. Phys.* **32**, 1335 (1993).

[3] R.M. Feenstra, J.A. Stroscio, J. Tersoff, A.P. Fein, *Phys. Rev. Lett.* **58**, 1192 (1987).

[4] T. Hasegawa, M. Nantoh, S. Heike, A. Takagi, H. Ikuta, K. Kitazawa, M. Kawasaki, H. Koinuma, *Phys. Scr. Vol. T* **49**, 215 (1993).

[5] K. Ikeda, K. Takamura, R. Iti, N. Koshizuka, *J. Vac. Sci. Technol. B* **10**, 2311 (1992).

[6] H. Murakami, R. Aoki, *J. Phys. Soc. Japan* **64**, 1287 (1995).

[7] Ch. Renner, O. Fischer, *Phys. Rev. B* **51**, 9208 (1995).

[8] C.K. Shih, R.M. Feenstra, G.V. Chandrashekhar, *Phys. Rev. B* **43**, 7913 (1991).

[9] E.L. Wolf, A. Chang, Z.Y. Rong, Yu.M. Ivanchenko, Farun Lu, *J. Supercond.* **7**, 355 (1994).

[10] A.P. Fein, J.R. Kirtley, R.M. Feenstra, *Rev. Sci. Instrum.* **58**, 1806 (1987).

[11] R.C. Dynes, V. Narayanamurti, J.P. Garno, *Phys. Rev. Lett.* **41**, 1509 (1978).

[12] D. Pines, *Physica C* **235-240**, 113 (1994).

[13] Z.-X. Shen, D.S. Dessau, B.O. Wells, D.M. King, W.E. Spicer, A.J. Arko, D. Marshall, L.W. Lombardo, A. Kapitulnik, P. Dickinson, S. Doniach, J. DiCarlo, A.G. Loeser, C.H. Park, *Phys. Rev. Lett.* **70**, 1553 (1993).

[14] J. Liu, Y. Li, C.M. Lieber, *Phys. Rev. B* **49**, 6234 (1994).

[15] T. Ekino, J. Akimitsu, *Frontiers in Solid State Sciences*, Vol. 1, World Scientific, Singapore 1992.

[16] J.G. Simmons, *J. Appl. Phys.* **34**, 238 (1963).

[17] W.F. Brinkman, R.C. Dynes, J.M. Rowell, *J. Appl. Phys.* **41**, 1915 (1970).

[18] T. Hasegawa, M. Nantoh, H. Ikuta, K. Kitazawa, *Physica C* **185-189**, 1743 (1991).

[19] Ch. Renner, O. Fischer, *Physica C* **235-240**, 53 (1994).

[20] M. Grajcar, A. Plecenik, P. Seidel, A. Pfuch, *Phys. Rev. B* **51**, 16185 (1995).